Cell Reports
Physical Science

Article

Iron as a key contributor in stability investigations of alkaline water electrolysis electrodes

Graphical abstract

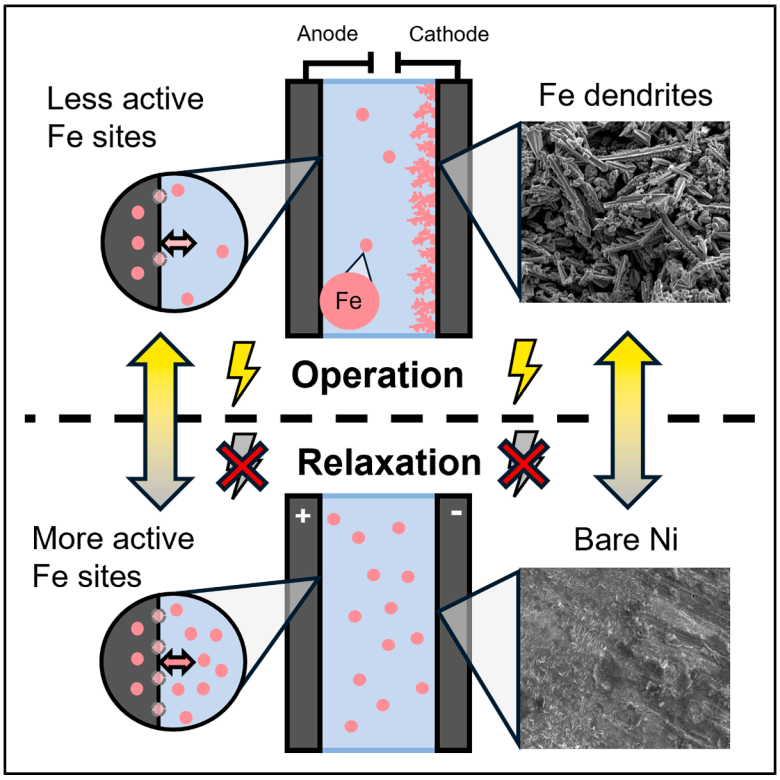

Highlights

- Dissolved Fe deposits on the cathode during operation and leaches back during shutdown
- Some Fe incorporates into the anode, while some Fe interacts dynamically at the surface
- Beyond short-term activity, dynamic Fe interactions contribute to long-term performance

Authors

Niklas Thissen, Yashwardhan Deo, Harol Moreno Fernández, Vera Seidl, Jan P. Hofmann, Anna K. Mechler

Correspondence

niklas.thissen@avt.rwth-aachen.de (N.T.),
anna.mechler@avt.rwth-aachen.de (A.K.M.)

In brief

Thissen et al. report a comprehensive study on how dissolved Fe interacts with alkaline water electrolysis electrodes during extended operation and shutdown. These interactions critically influence electrode activity and stability, offering important insights for understanding electrolyzer performance and guiding the development of improved electrode materials.

Thissen et al., 2026, Cell Reports Physical Science 7, 103138
March 18, 2026
https://doi.org/10.1016/j.xcrp.2026.103138

CellPress

Cell Reports
Physical Science

CellPress
OPEN ACCESS

Article

Iron as a key contributor in stability investigations of alkaline water electrolysis electrodes

Niklas Thissen,[1,*] Yashwardhan Deo,[1] Harol Moreno Fernández,[2] Vera Seidl,[1] Jan P. Hofmann,[2] and Anna K. Mechler[1,3,*]
[1]Electrochemical Reaction Engineering (AVT.ERT), RWTH Aachen University, Aachen, Germany
[2]Surface Science Laboratory, Department of Materials and Geosciences, Technical University of Darmstadt, Darmstadt, Germany
[3]Lead contact
*Correspondence: niklas.thissen@avt.rwth-aachen.de (N.T.), anna.mechler@avt.rwth-aachen.de (A.K.M.)
https://doi.org/10.1016/j.xcrp.2026.103138

SUMMARY

Alkaline water electrolysis (AWE) holds great potential for sustainable hydrogen production. However, further industrially relevant research is crucial for bridging the gap toward industrial application. Here, one important aspect is the understanding and improvement of the stability of AWE electrodes under high current densities. In this context, we report that dissolved iron (Fe) in the electrolyte, besides enhancing the short-term performance of nickel (Ni)-based electrode materials, significantly affects their stability. We demonstrate that, during operation, Fe is deposited on the cathode, whereas during shutdown, it leaches back into the electrolyte. This reversible Fe-deposition process significantly enhances the long-term performance of cathodes in high Fe-containing systems (>10 ppm). Ni anodes, concurrently, undergo a reversible deactivation over operation time as fewer Fe sites are available to establish the dynamic Fe-Ni equilibrium. Hence, dissolved Fe significantly affects the Ni-electrode stability, which is an often-overlooked aspect in catalyst research.

INTRODUCTION

Alkaline water electrolysis (AWE) represents a highly promising technique for green hydrogen production.[1,2] As noble metal catalysts are not necessarily required, a cost-efficient upscaling is enabled due to low investment costs.[3,4] Nevertheless, poor kinetics affect the oxygen evolution reaction (OER) adversely, and high Tafel slopes for the hydrogen evolution reaction (HER) prevent low-cost AWE systems from operating efficiently at high current densities. Therefore, efficient electrocatalysts are essential to facilitate both reactions.[5–8] In this context, the role of dissolved iron (Fe) in the electrolyte has gained considerable attention, as it influences the performance of both HER and OER for nickel (Ni)-based electrocatalysts significantly.[9–12] From an industrial perspective, the effect of Fe is of particular interest, given that some amount of Fe is invariably present in low-cost electrolyzer systems due to the steel periphery.[13]

For Ni cathodes, an effect of Fe has already been proposed by Riley et al. in 1986.[14] The authors showed that by adding 3 ppm of Fe to the electrolyte, an improved stability was achieved under mild conditions. The cathodic degradation mechanism in low Fe-containing systems was later referred to as Ni-hydride formation, which leads to an increased hydrogen flux. This mechanism may be inhibited in high Fe-containing systems.[15,16] A similar improvement, reported by Mauer et al., can be observed when Fe is directly incorporated into the cathode.[10] In addition, authors report an activity enhancement owing to the deposition of Fe needles in high Fe-containing electrolytes, increasing the active surface area of bulk materials.[17–19]

For Ni-based anodes, the role of Fe in OER was systematically investigated considerably later, and the exact mechanisms are still being debated. Here, Fe might act as a co-catalyst through synergistic interaction with the main catalytic material or may actually function as the main active site itself while being hosted by the remaining material (e.g., Ni).[20,21] Irrespective of the actual mechanism, the addition of Fe significantly improves the performance of Ni- or Co-based catalysts.[9,22] Fe can also inhibit excessive growth of the oxyhydroxide phase, preserving the electrode's electrical conductivity.[23] As for the cathode, both Fe in the electrolyte and in the electrode have been shown to increase the anodic activity.[24] However, the role of Fe in enhancing anode stability was addressed only recently. It was reported that, to achieve stable operation, Fe should be in a dynamically stable state as a result of simultaneous dissolution and redeposition on the electrode.[25,26] Hence, several studies focus on enhancing this equilibrium, e.g., by catalyzing the redeposition process using Co or reducing Fe dissolution through protective layers.[27–29]

From an industrial perspective, and as several authors emphasize, the effect of Fe needs to be thoroughly investigated under applied conditions. This is particularly important because Fe is much less stable in such harsh environments (80°C, 30 wt % KOH).[12,20,30] A recent study by Demnitz et al. provided a first overview of the Fe effect under near-industrial conditions, reinforcing its beneficial effect on electrode activity.[31] Interestingly,

the authors did not observe an optimal Fe concentration, as the highest content of ~6 ppm led to the highest activity for both HER and OER. The extent of the Fe's influence on the system's stability in long-term measurements, however, remains unexplained. This is especially true when considering transient loads, which are currently suspected to be the main cause of degradation in AWE.[32–34]

In this study, we examine how Fe influences the stability of Ni-based electrodes in AWE under industrial conditions. In particular, we investigate the Fe distribution in the electrolyte and on the electrodes during operation and shutdown. Electrolyte samples were analyzed using inductively coupled plasma optical emission spectroscopy (ICP-OES), while both electrodes were examined using scanning electron microscopy coupled with energy-dispersive X-ray spectroscopy (SEM-EDX) and X-ray photoelectron spectroscopy (XPS).

RESULTS

Fe distribution in intermittent operation

This study investigates four initial Fe concentrations in the electrolyte. The lowest concentration of 0.2 ppm Fe displays the natural intrinsic impurities from KOH production. Additionally, higher Fe-containing electrolytes with 1, 10, and 50 ppm were prepared by adding dissolved $Fe(NO_3)_3$ to the respective batches. Please note that the addition of 50 ppm Fe to the electrolyte exceeds the solubility limit, which is reported to be in the range of 15–20 ppm at the given industrially relevant conditions (80°C, 30 wt % KOH).[12,35] We first analyze and discuss the effect of the dissolved Fe as a function of the operating mode using various analysis techniques for both the electrodes and the electrolyte. Based on this, we contextualize the electrodes' performances and draw inferences for future catalyst testing.

To investigate the Fe distribution in intermittent operation, we operated an electrochemical beaker cell under industrially relevant conditions (1 A cm^{-2}, 80°C, 30 wt % KOH) for 50 h and subsequently shut it off for 4 h.[36] During both operation and consecutive relaxation, we monitored the Fe concentration by sampling and analyzing the electrolyte via ICP-OES at fixed intervals of 0, 2, 4, 24, and 50 h (see Figure 1A). The analysis reveals that the Fe concentration in the electrolyte undergoes a drastic exponential decrease by 97%–99% over the 50 h operation time for all four initial Fe concentrations (50 ppm to 400 ppb; 10 ppm to 60 ppb; 1 ppm to 15 ppb; 0.2 ppm to 6 ppb). Thus, only a minimal amount of 1%–3% of the initial Fe remains in the electrolyte. During the subsequent 4-h relaxation phase, however, a considerably faster increase of the Fe concentration takes place. Indeed, for the lowest Fe-containing system (0.2 ppm), the initial Fe concentration is reestablished within 1 h, whereas for the 1 and 10 ppm Fe experiments, 2 and 4 h are required, respectively. For the highest Fe-containing system (50 ppm), the initial concentration was not reobtained within the 4-h relaxation period and remains 40 ppm below the initial value.

In addition to the Fe concentration in the electrolyte, the electrodes were investigated for Fe incorporation or deposition, using SEM-EDX. Figure 1B depicts the mass ratio of Fe on the electrodes before and after relaxation, i.e., after 50 h chronopotentiometry (CP) and 50 h CP + 4 h open circuit potential (OCP), respectively, obtained by multipoint EDX mapping technique. In all cases, anodic Fe incorporation was undetectable, whereas significant amounts of Fe were obtained on the cathodes. The respective cathodic Fe mass ratios after 50 h of operation increase with the initial Fe concentration and account for 9 wt % (0.2 ppm), 29 wt % (1 ppm), 39 wt % (10 ppm), and 42 wt % (50 ppm). After relaxation, the Fe mass loads display a significant but not an absolute decrease in Fe mass ratio to 1 wt % (0.2 and 1 ppm) and 14 wt % (10 ppm). This suggests that the decrease in dissolved Fe in the electrolyte primarily correlates with a cathodic deposition process, while the increase of Fe in the electrolyte during relaxation originates from a cathodic leaching process. For the highest Fe-containing system (50 ppm), however, the cathode's Fe mass load is unchanged after relaxation, which implies that the leaching process is impaired as the solubility limit of Fe in the electrolyte is reached. Albeit, this solubility limit does not prevent the cathode from absorbing significantly more Fe beforehand, as initially undissolved Fe, which may precipitate during electrolyte preparation, can continuously redissolve into the electrolyte and ultimately deposit on the cathode during the operation.[30]

SEM investigations reveal that, in low Fe-containing systems, the cathodes exhibit a relatively uniform morphology; small spherical deposits with a mean diameter of 10–100 nm partly cover the Ni mesh (Figure S1). Remarkably, for electrolyte batches containing both Fe and other metal impurities (e.g., Cu, Zn, and Pb), we observed co-deposition of the respective metals, which contribute to the cathodes' metallic composition (Figure S2). After relaxation, the cathodes from the low Fe-containing system show no deposits (Figure S3); most of the Fe and also other co-deposited metals are redissolved into the electrolyte upon relaxation.

For the high Fe-containing systems, two different deposition zones can be observed: a relatively uniform, low Fe-containing zone on the smooth front surfaces of the expanded Ni mesh and a significantly more porous, high Fe-containing zone on the recessed parts (e.g., angled surfaces and edges), revealing a dendritic pattern (Figure 1C). The dendrites grow up to a mean diameter of ~1 μm and a length of ~10 μm and consist almost entirely of Fe (EDX in Figure S4). In contrast, the homogeneous deposition on the front surfaces contains 10–20 wt % Fe, indicating a much thinner deposition layer. This characteristic 2-zone deposition may be attributed to the mechanical instability of the Fe dendrites, which can break off easily on the smooth surfaces because of rising bubbles, while fewer bubbles access the recessed parts of the electrodes, and the dendrites are retained. Interestingly, after relaxation, the optical analysis reveals leftover Fe structures, which display a denser and more crystalline phase (Figure S5). This indicates that the deposition process during operation might initially be crystalline and becomes only subsequently dendritic owing to mass transport limitations of less available Fe in the electrolyte.

Since no anodic incorporation of the Fe was detected with the EDX technique, XPS analysis was employed, offering a high sensitivity for the detection of surface-limited Fe incorporation. Figure 1D displays the Fe/Ni + Fe mass ratio obtained from Ni 3p and Fe 3p spectra (Figure S6). XPS revealed significant

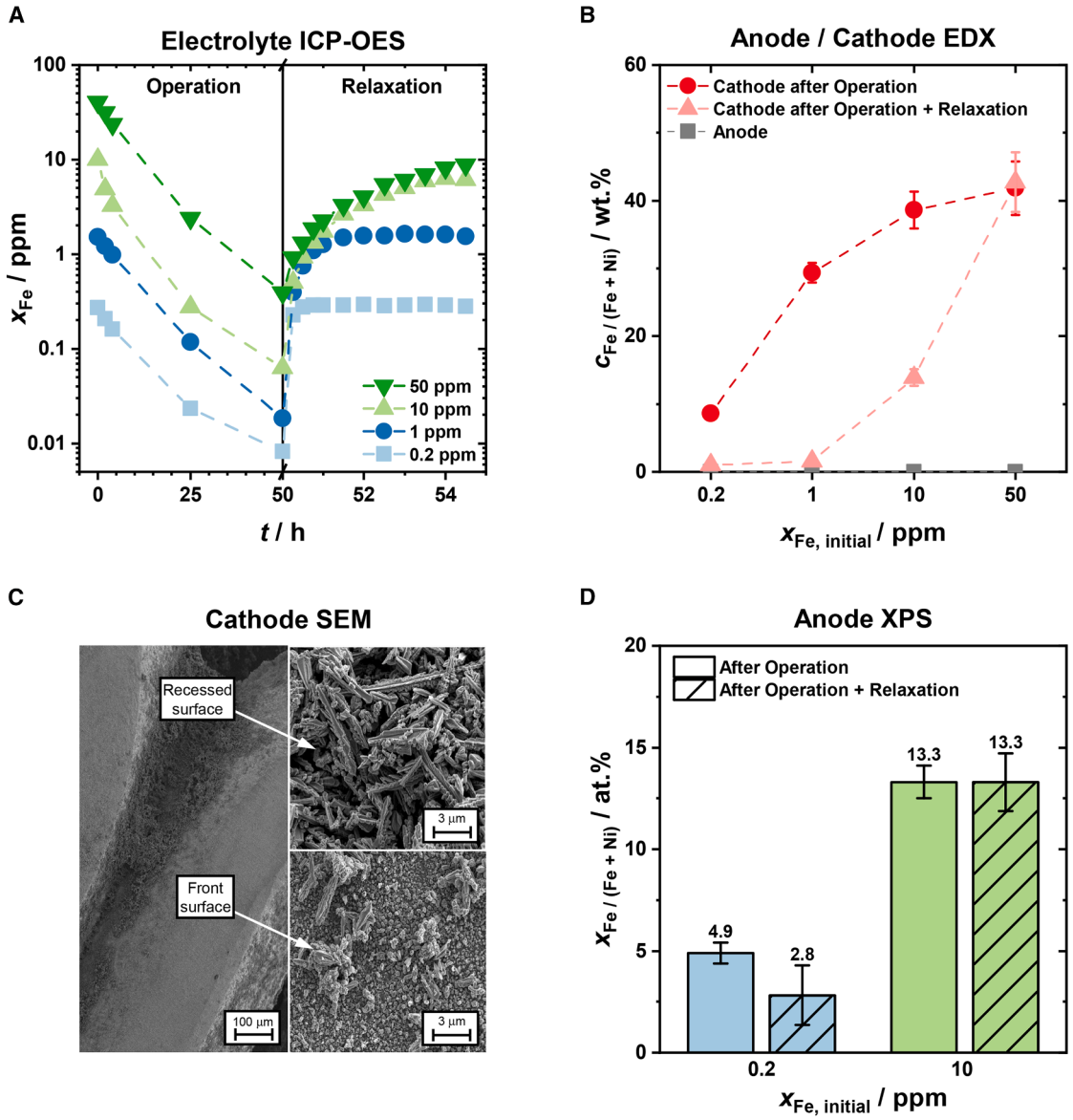

Figure 1. Analytical investigations of the electrolyte, anode, and cathode to understand the Fe distribution in intermittent operation

(A) Fe concentration in the electrolyte at fixed time intervals analyzed by ICP-OES during constant current operation at 1 A cm^{-2} (left) and during consecutive relaxation (4 h of OCP, right) for 4 different initial Fe concentrations.

(B) Mass fraction of Fe/(Fe + Ni) in surface investigations obtained by multipoint EDX mapping of anode and cathode before (50 h CP) and after relaxation (50 h CP + 4 h OCP) for 4 different initial Fe concentrations.

(C) SEM images of two different types of cathodic Fe deposits obtained after 50 h CP with 10 ppm initial Fe concentration. Displayed are an electrode overview (left, 50×; scale bars, 100 µm) and magnified images of a high dendritic area on the recessed surface (top right, 5,000×; scale bars, 3 µm) and a more uniform area on the front surface (bottom right, 5,000×; scale bars, 3 µm).

(D) Anodic Fe incorporation determined by XPS displayed for anodes analyzed after operation (50 h CP) and after consecutive relaxation (50 h CP + 4 h OCP) for two initial Fe concentrations (0.2 and 10 ppm). For the corresponding spectra, see also Figure S6. Data are represented as mean ± SEM.

amounts of Fe on the surface of the anodes after operation, which increases with higher Fe content in the electrolyte from 5 atom % (0.2 ppm) to 13 atom % (10 ppm). After the 4 h relaxation phase, the Fe content does not change significantly, suggesting an irreversible Fe incorporation in this regime. Fe might be incorporated either as $NiFe(OH)_2$ or an *in situ* formed layered double hydroxide (LDH).[37–39] Under OER conditions, however, both species are expected to transition into an oxyhydroxide phase. Interestingly, electrodes exposed solely to 30 wt % KOH at 80°C without an applied current exhibited slightly higher Fe content, accounting for 8 atom % (0.2 ppm) and 21 atom % (10 ppm). This indicates that Fe incorporation (1) also occurs without external electrical driving force and (2) may be even inhibited by an applied current, possibly because of the overall

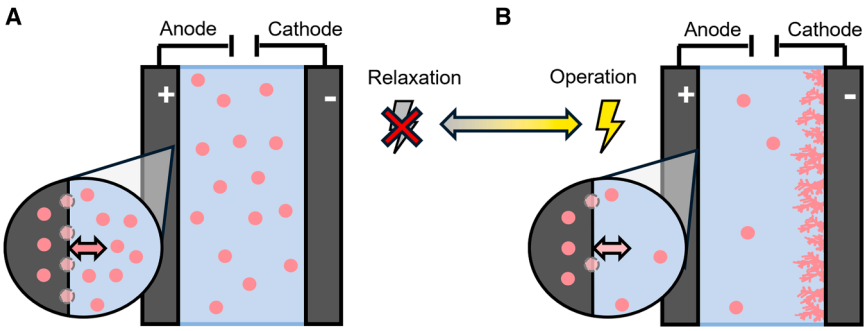

Figure 2. Dynamic model of Fe distribution in a simplified electrolyzer setting

Schematic representation of the hypothesized Fe distribution during relaxation (A) and operation (B) in a simplified AWE electrolyzer (no diaphragm, mixed electrolyte). Local resolution of the anodic environment indicates an irreversible Fe incorporation and a dynamic equilibrium between dissolved Fe in the electrolyte and adsorbed topical Fe on the electrode. During operation, Fe deposition causes the build-up of porous cathodic structures and a shift in the dynamic Fe equilibrium at the anode.

decrease of Fe in the electrolyte during operation (*vide supra*). This, however, does not apply to alternating instead of constant loads. Here, much higher Fe contents—up to 29 atom %—were observed for the 10 ppm system (Figures S7 and S8). This aligns with the findings from the literature, which suggest that potential cycling significantly affects anodic Fe incorporation.[26,40,41] Additionally, we hypothesize that, beyond irreversibly incorporated Fe, a fraction of reversibly bound surface Fe exists in dynamic equilibrium with Fe species in the electrolyte. This labile surface Fe is believed to play a pivotal role in electrocatalytic activity, yet remains undetectable by *ex situ* XPS (*vide supra*).

The dynamic behavior of Fe also correlates with existing thermodynamic data. OCP analysis reveals that, within the 4 h relaxation and leaching period, high Fe cathodes remain below 0 V vs. reversible hydrogen electrode (RHE), whereas low Fe cathodes quickly increase in potential to ~800 mV vs. RHE (Figure S9). Thus, Fe leaching already occurs below 0 V vs. RHE, where, according to Pourbaix diagrams, $HFeO_2^-$ species are thermodynamically favored.[42] Additionally, Pourbaix diagrams at elevated temperatures predict the formation of ionized hydroxide species, such as $Fe(OH)_4^{2-}$ or $Fe(OH)_3^-$.[43] When returning to more cathodic potentials during HER, metallic Fe is redeposited.[42,43]

On the basis of various analysis techniques, we hypothesize a mechanistic model for the Fe distribution in intermittent AWE (Figure 2). Herein, the Fe is dynamically distributed depending on the operation mode of the cell. During constant current operation, the Fe is continuously deposited from the electrolyte onto the cathode, where, in relation to its concentration, homogeneous, dendritic, and/or crystalline Fe structures are formed. The dynamic equilibrium on the anode surface simultaneously shifts toward lower Fe as there is less Fe available in the electrolyte. The mechanism is reversed during relaxation, resulting in a leaching of the cathodic deposits and an increase in dissolved Fe in the electrolyte with subsequent effects on the anode. Please note that the mechanisms presented were observed in a beaker cell setup using 1 cm^2 electrodes in 220 mL of electrolyte. Changing the experimental setup—especially the cell geometry—could significantly alter the observed timescales of deposition and redissolution.

Electrochemical performance

Dissolved Fe in the electrolyte interacts with the Ni anode surface and, additionally, deposits on the cathode. This interaction, however, changes significantly during shutdown (*vide supra*). In the following, we investigate the effect of dissolved Fe on the electrochemical stability of Ni mesh electrodes during intermittent operation. Therefore, we operated the cell for 50 h at 1 A cm^{-2}, interrupted the operation by a 4 h relaxation phase, and proceeded with another 50 h of operation (Figure 3). For reference, the non-*iR*-corrected potential is reported in Figure S10.

The cathodic potentials are displayed in Figure 3A. The overall cathodic performance improves with increasing Fe concentration. This is, on one hand, reflected by the initial activity, which is 70 mV worse for low Fe-containing electrolytes (0.2 & 1 ppm) compared to the highest Fe-containing one (50 ppm), with an initial overpotential of only 370 mV. Interestingly, this trend also translates to the stability of the samples. Cathodes in high Fe-containing electrolytes (10 & 50 ppm) activate for ~70 mV each over the course of 10 h and provide cathodic potentials of –360 and –310 mV vs. RHE, respectively, at the end of the first 50 h operation phase.

On the other hand, cathodes in low Fe-containing electrolytes (0.2 & 1 ppm) remain at the inferior potential and show little activation of <20 mV. The different trends of both high and low Fe-containing electrolytes correspond to the cathodic Fe incorporation and deposition mechanisms discussed in the previous chapter. In high Fe-containing systems, porous Fe deposits induce a high active surface area, facilitating the efficient operation at challenging current densities of 1 A cm^{-2}. In contrast, the resulting lack of Fe implies a lower surface area and, therefore, fewer active sites. Another intensifying effect on the poor performance of the Ni cathodes in the low Fe-containing systems was observed when using an impure electrolyte batch containing significant amounts of Cu, Zn, and Pb. Herein, the co-deposition of the other HER-inactive metals (especially Zn and Pb) resulted in a further deactivation to –700 mV vs. RHE (Figure S11). Remarkably, the potential of the Ni cathode in purified electrolyte, with significantly less Fe of <7 ppb, quickly drops to –1.20 V vs. RHE within the first 5 h of measurement (Figure S12), further indicating a poor intrinsic stability of Ni cathodes without Fe. Mauer et al. attributed the cathodic degradation mechanism to the formation of NiH, which may be prevented in the presence of high amounts of Fe in the system.[10]

After the 4 h relaxation, the cathodic performance for all Fe concentrations partly decreases, after which the cathodes are reactivated again and provide a similar trend compared to the first 50 h of measurement. This relates to the formerly

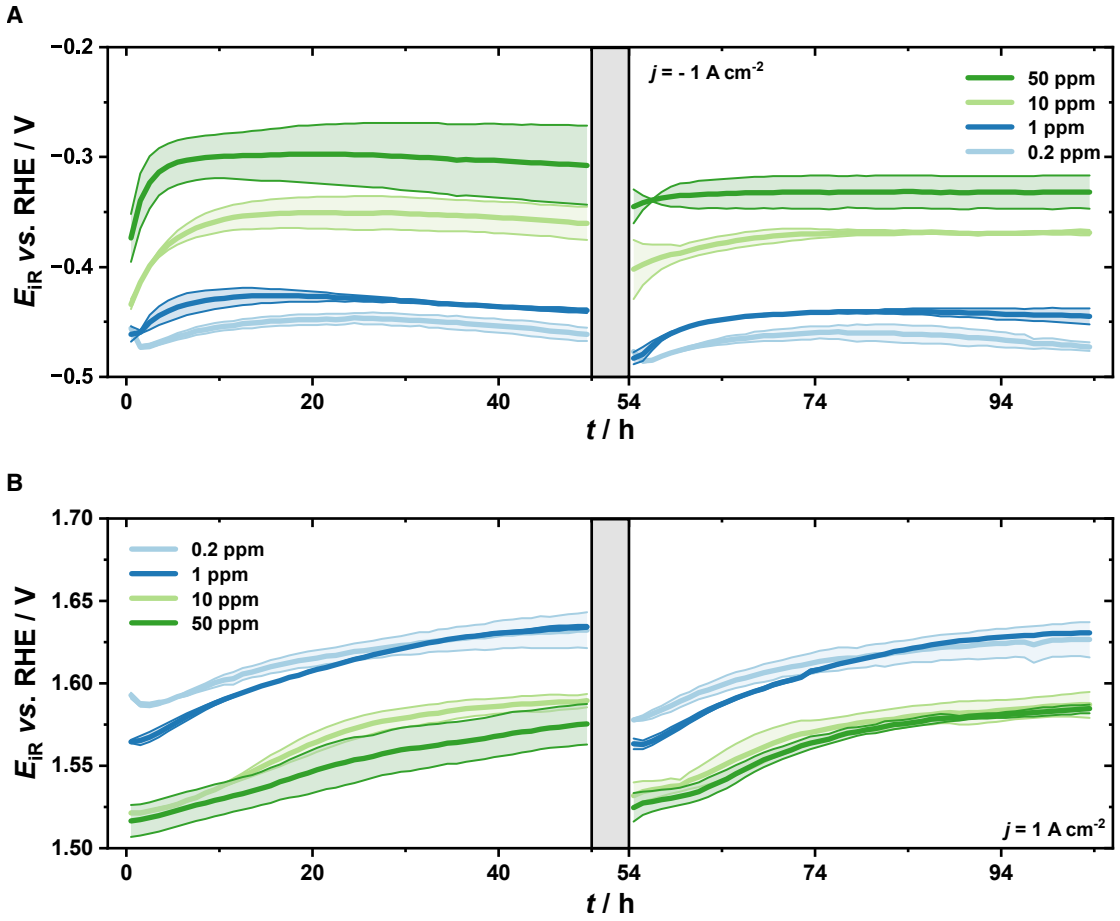

Figure 3. Electrochemical stability of Ni electrodes in dependence on Fe concentration

Chronopotentiometric measurements (*iR*-corrected and averaged) at 1 A cm^{-2}, 80°C, and 30 wt % KOH for 100 h, including a 4 h relaxation after 50 h, for a 1 cm^2 Ni mesh cathode (A) and a 1 cm^2 Ni mesh anode (B). Different Fe concentrations in the electrolytes were used, accounting for 0.2 (light blue), 1 (dark blue), 10 (light green), and 50 ppm (dark green). Data are represented as mean ± SEM.

observed Fe leaching (Figure 1B), resulting in a worse initial performance and subsequent slight increase, as Fe deposits, which were leached into the electrolyte during relaxation, are reassembled.

The observed cathodic trend also translates to accelerated durability tests (ADTs, Figure S13). Herein, cathodes exhibit significantly improved activity in high Fe-containing electrolytes; however, no noticeable impact on degradation is observed. Longer constant current measurements demonstrate that bare Ni cathodes operate with high stability and the potential shift between high and low Fe-containing electrolytes remains approximately 90 mV, even after 300 h (Figure S14). Interestingly, this trend could not be extended to industrial noble metal-coated cathodes. These cathodes perform 30 mV worse under high Fe conditions (∼–150 mV vs. RHE), presumably because the high catalytic activity of the noble metal catalyst is poisoned by Fe. However, despite the slight reduction in performance due to Fe presence, the advantage vs. bare Ni remains significant (220 mV), and the performance stability is not affected by Fe presence during the test.

The anodic potentials are displayed in Figure 3B. With increasing Fe concentration in the electrolyte, a significant decrease in anodic overpotential is observed. The initial potentials improve with increasing Fe concentration in the electrolyte from 1.60 V vs. RHE (0.2 ppm) to 1.56 V vs. RHE (1 ppm) and 1.52 V vs. RHE (10 and 50 ppm). This trend is also consistent with existing literature, as significant enhancements in OER activity owing to dissolved Fe have already been reported under both laboratory and industrial conditions.[9,31] In addition, we herein demonstrate that no further improvement can be achieved when further increasing the Fe concentrations from 10 ppm to, e.g., 50 ppm, likely because the solubility limit is reached beforehand. During the subsequent stability measurement, deactivation is observed, which increases from low Fe-containing systems with 40 mV of deactivation to high Fe-containing systems with 70 mV of deactivation. The deactivation slope reduces toward the end of the 50 h CP, implying a more stable operation hereafter. Interestingly, when using Fe-purified electrolyte (<7 ppb Fe), a poor initial activity (1.81 V vs. RHE) is followed by an activation of 150 mV, approximating

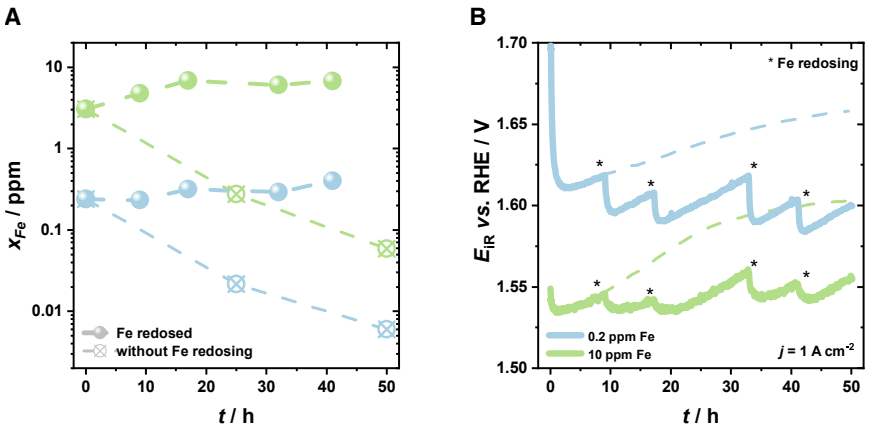

Figure 4. *In situ* Fe redosing to prevent anode deactivation

(A) ICP-OES analysis of electrolyte samples taken from chronopotentiometric measurements (1 A cm^{-2}) for 50 h with initial Fe concentrations of 0.2 ppm (blue) and 10 ppm (green). Throughout the experiment, the initial Fe concentrations were restored twice daily (solid circle). Reference experiments (without Fe redosing) are represented by the light crossed-out dots.

(B) Corresponding anodic potentials for the redosed systems (solid line) and the reference system without Fe redosing (dashed line). Data are represented as mean ± SEM.

the performance in the Fe-containing systems after 50 h (Figure S15). Thus, Fe in the electrolyte might not necessarily be a prerequisite to enable the stability of Ni anodes under industrial conditions.

After 4 h of relaxation at OCP, a recovery of the initial anodic performance was observed for all four Fe concentrations. This reactivation is then, however, followed by another deactivation comparable to the first 50 h CP. A similar behavior was also observed for different materials in other studies.[44–46] The decrease in the anodic performance consequently occurs mainly as reversible deactivation, for which we propose the following mechanism: a dynamic Fe equilibrium between the anodic surface and the electrolyte is established, and the electrode activity is directly correlated to the amount of Fe in the electrolyte. During operation, most of the Fe in the electrolyte is deposited on the cathode within a few hours, which not only enhances the cathodic activity by creating active deposits but also decreases the anodic performance by shifting the dynamic Fe equilibrium at the anode toward lower Fe content. Please note that a portion of Fe remains irreversibly incorporated (*vide supra*) but appears to contribute less to the activity compared to the dynamically adsorbed and desorbed Fe. During the subsequent relaxation, the process is reversed, allowing the Fe to redissolve in the electrolyte and reestablish the anodic activity.

To further validate this hypothesis, we conducted experiments in which the Fe concentration was reestablished at regular intervals during operation (for 0.2 and 10 ppm of initial Fe content) by regular redosing with $Fe(NO_3)_3$. The corresponding Fe concentration over time is displayed in Figure 4A. A constant Fe concentration in the electrolyte translates to a more stable anodic performance (Figure 4B). A sharp reactivation was achieved whenever Fe was redosed, and the deactivation could be reversed for both low and high Fe-containing systems. In fact, for the low Fe-containing (0.2 ppm) system, the anode displays a slight activation ($\sim$0.5 mV h^{-1}) likely because of surface oxidation or further Fe incorporation. In contrast, the anodic potential remains constant in the high Fe-containing system (10 ppm). Concluding the results discussed, we unraveled a mechanism behind anodic deactivation by separating the effects of operation time and Fe concentration in the electrolyte.

The effect described is also reflected in ADTs (Figure S16). Here, the initial performance difference is largely maintained, with no observable deactivation—presumably because Fe is repeatedly leached during the shutdown phases of the protocol, thereby reestablishing the dynamic Fe equilibrium. However, similar to the cathode, the ADT does not induce additional degradation, as bulk Ni remains highly stable. Constant long-term measurements over 300 h further show that the initially beneficial effect of the high Fe-containing electrolyte runs out after approximately 100 h, after which both electrodes exhibit comparable performance (Figure S17). Moreover, the observed trend for the Ni anode can be effectively transferred to the catalyst-coated industrial electrode. Analogously, an initially significant performance boost induced by Fe is observed, which, however, diminishes substantially over time.

True anodic performance can, therefore, be determined through longer constant current measurements or via Fe-redosing, both of which are either highly resource-intensive or impractical and inaccurate. Therefore, we propose an electrochemical protocol, which we term the Relax Protocol—designed for anodic stability measurements and addressing the Fe-related reversible deactivation. Herein, the operation is deliberately interrupted in regular intervals of 10 h with a 4 h relaxation phase to allow for cathodic Fe leaching and, hence, establish the initial Fe concentration (Figure 5A). To assess the anode's stability, its performance can now be compared at different time points, which correspond to similar Fe concentrations. This offers a more reliable anodic characterization compared to conventional protocols. Figure 5B illustrates a comparison for the anodic stability of Ni in 10 ppm Fe-containing electrolyte between the standard CP and the Relax Protocol. While the standard CP protocol shows a degradation of 70 mV within 40 h of measurement, the Relax Protocol reveals only an insignificant degradation of less than 10 mV over the course of the experiment.

Combining the findings of the anodic stability characterization, we observe similar deactivation over the entire Fe range. This phenomenon can be related almost exclusively to the decrease in dissolved Fe during operation and the corresponding shift in the dynamic Fe equilibrium with the anode surface. Thus, a significant irreversible anodic degradation could not be proven for

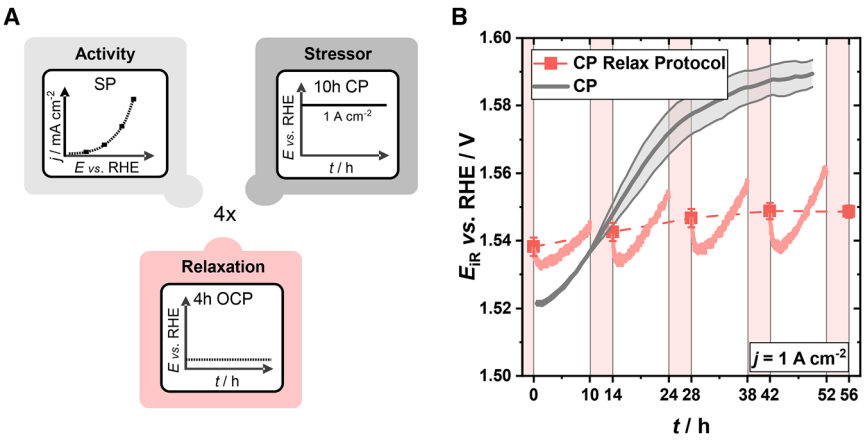

Figure 5. Relax Protocol for improved understanding of OER stability

(A) Schematic representation of the proposed Relax Protocol, including an activity measurement in the form of a stationary polarization, followed by a stressor (in this case, a 10 h CP) and a relaxation step for 4 h to reestablish the initial Fe concentration in the electrolyte. These steps are looped at least four times.

(B) Comparison of regular CP measurement at 1 A cm^{-2} with and without the Relax Protocol for a 10 ppm Fe system. Data are represented as mean ± SEM.

any initial Fe concentration. In fact, when applying longer constant current protocols (e.g., 300 h), the initial performance boost of dissolved Fe diminishes over time and the anodic performance is comparable and stable for both low and high Fe hereafter.

DISCUSSION

Dissolved Fe in the electrolyte enhances the performance of Ni-based cathodes by Fe deposition. Here, a high Fe content in the electrolyte is a key requirement for enabling bare Ni cathodes to provide a stable long-term performance at high current densities, causing a performance increase of up to 150 mV at 1 A cm^{-2}. Contrarily, for the OER, we demonstrate that the initial activity is enhanced in high Fe-containing systems by up to 80 mV, yet this performance boost eventually runs out after 100 h of operation. Considering relaxation, we did not encounter irreversible anodic degradation for the entire Fe range, suggesting that Fe is not an ultimate prerequisite to enable stable anodic performance. Yet, the observed activity of anodes can strongly depend on the dynamic equilibrium of Fe dissolved in the electrolyte and, hence, directly interacts with the processes at the cathode.

When moving from bulk Ni electrodes to synthesized catalyst-coated electrodes, the amount of dissolved Fe needs to be chosen carefully and adapted to the selected electrodes, especially with regard to the cathode. It should be kept in mind that the Fe deposition process partly covers the electrode and, therefore, might compromise the superior performance of the catalyst underneath. For instance, when high-performing noble metal-based catalysts (e.g., Pt and RuO_2) are used on cathodes, electrode manufacturers may have to limit the amount of dissolved Fe to guarantee long-term performance.[47,48] This also translates into economic aspects, as a high Fe concentration in the electrolyte allows for using low-cost steel peripheries, which inherently lead to high Fe leaching. In such a case, however, the continuous Fe leaching could lead to progressive thickening of the Fe layer, which could become critical over time. Though for selected catalysts requiring low Fe concentrations, special alloys or high-performance plastic periphery must be used, which is either cost-expensive or not pressure-resistant.[13]

These considerations should also be reflected in academic research, and the effect of dissolved Fe needs to be considered during electrode development and testing. For cathodes, we illustrate the deposition process of Fe but also of other trace metals originating from the electrolyte (e.g., Cu, Zn, and Pb). Here, a systematic study of interferences between different contaminants could be fruitful.[49,50] Accordingly, tests in low Fe-containing electrolytes to determine the intrinsic activity of new materials are reasonable. On the other hand, our study suggests that, for non-precious metal Ni-based catalysts (e.g., NiCu and NiMo), kinetic synergies with dissolved Fe might still be beneficial and should be investigated. It is important to note here that synthesized cathodes should be benchmarked to the performance of run-in (e.g., after 10 h CP) Fe-deposited Ni cathodes, as these represent a cost-effective electrode in high Fe-containing systems with a relatively low overpotential of 330 mV at 1 A cm^{-2}.

In the field of anode research, it should be noted that the initial activity of Fe-sensitive materials (e.g., Ni & Ni-based materials) is enhanced by dissolved Fe in the electrolyte. These materials also exhibit Fe-related reversible deactivation in stability measurements. An initial decrease in performance (e.g., 40–70 mV in the first 50–100 h), therefore, does not necessarily imply severe degradation but might be due to Fe interaction. This effect can be excluded by using the herein suggested Relax Protocol. In this context, it should be noted that Fe-containing anodes may behave differently compared to bare Ni, as the activity might not be as dependent on dissolved Fe. Yet, also for Ni-Fe electrodes, a dynamic Fe-concentration at the surface can be expected.[41] If Fe dissolution occurs from the Fe-containing anodes, it might initially appear to activate the anode due to an increased Fe-concentration in the electrolyte. The released Fe, however, will be deposited on the cathode, which again implies a complex interaction between cathode and anode behavior.

Overall, we could show the severe impact of Fe in the electrolyte on both anode and cathode performance under industrially relevant AWE conditions. Besides impacting the activity, the observed stability strongly depends on the dynamically developing Fe concentration in the electrolyte. This shows the importance of not only individually studying single electrode performances but also considering the electrolyte as a connecting element between the anode and cathode processes. Based on our insights, we suggest a relaxation protocol that enables the

analysis of irreversible anode degradation under constant Fe concentration. Furthermore, our insights can provide knowledge-based information on the mode of operation of real electrolyzers, not only considering the choice of electrode materials and electrolyte purities but also operation modes like electrolyte management and the possible impact of dynamic load changes. Further studies on these interactions under realistic environments are still necessary in the future.

METHODS

Electrochemical measurements

Our previous publication extensively discusses the beaker cell setup used for electrochemical investigations.[36] Herein, industry-standard Ni-expanded metal mesh (>98% purity) with a projected surface area of 1 cm^2 (i.e., outer circumference of $\sim 8 \times 12$ mm) was used as anode and cathode, respectively. Please note that the corresponding geometric 3D surface area is roughly 1.5 cm^2 (i.e., front, back, and edges). Tests on the industrial catalyst-coated electrodes were carried out using a DSA A1-expanded mesh anode and a Ni Flynet-activated NRG (De Nora). The PTFE beaker was filled with pre-mixed 30 wt % KOH (Bernd Kraft), providing an overall Fe concentration of 0.2 ppm (determined by ICP-OES). For experiments with higher Fe concentration, a Fe standard solution with 1 g L^{-1} Fe in 5% HNO_3 (Agilent) was added to the heated electrolyte accordingly. KOH was exclusively stored and prepared in polymer equipment (e.g., polypropylene, PTFE) in order to eliminate impurities leaching from standard glassware. A VSP-3e potentiostat from Bio-Logic SAS and the accompanying EC-Lab V11.46 software from the same provider were used to apply and implement the electrochemical protocol. As reference electrodes, miniRHEs, supplied by Gaskatel, were used. To ensure proper functionality of the miniRHEs, calibration measurements, according to Jerkiewicz et al., were carried out on a weekly basis.[51] The electrochemical protocols were conducted as described in the manuscript, after a preconditioning step at 100 mA cm^{-2} with a consecutive relaxation step (4 h each). All experiments were repeated at least once; statistical significance is shown as the standard error of the mean. Accelerated durability tests were performed based on the stressor from Tsotridis et al. and incorporated into the Relax Protocol framework (i.e., repeated 10 h ADT, 4 h OCP).[52]

Analytical techniques

SEM and EDX

A Hitachi Schottky SU5000 FESEM was used to study the microstructure of the Ni mesh electrodes. Images were taken in the secondary electron (SE) mode at a magnification of 100×, 500×, 1,000×, 5,000×, 10,000×, and 20,000× at an accelerating voltage of 5 kV. A Bruker EDX, coupled to the SEM, was used to obtain the elemental compositions of the electrodes. The accelerating voltage of the electrons was changed to 15 kV for the EDX analysis.

XPS

For XPS measurements, a Thermo Fisher Escalab 250 spectrometer implemented at the DAISY-SOL cluster tool was used. It is equipped with an Al Kα X-ray source (monochromatic Thermo Fisher XR6, $h\nu = 1486.74$ eV). Survey and high-resolution spectra were measured in fixed analyzer transmission mode with a pass energy of 50 eV (step size of 0.5 eV) for the survey and 20 eV (step size of 0.05 eV) for the core levels. The system was calibrated to 0.00 eV binding energy of the Fermi level of sputter-cleaned Ag as well as to the emission lines of Au $4f_{7/2}$ at 83.98 eV, Ag $3d_{5/2}$ at 368.26 eV, and Cu $2p_{3/2}$ at 932.67 eV binding energy with deviations ≤ 0.1 eV. The data analysis was performed with CasaXPS, version 2.3.22.[53] Handbooks of monochromatic XPS spectra were used to identify the metal or metal oxide species from the peak positions.[54,55]

ICP-OES

An Agilent 5800 VDV ICP-OES was used to measure the Fe concentration in the KOH of the samples, which was taken before, during, and after OER experiments. For this, all samples were diluted by a factor of 1:10, resulting in a concentration of 3 wt % KOH. The instrument was initially calibrated using a standard addition method, wherein the calculated amounts of a Fe standard solution were added to a reference 3 wt % KOH solution, and the resulting intensities from the ICP-OES were used to obtain a calibration curve. Axial viewing and automatic background correction were employed. The Fe signal was detected at wavelengths of 238.204 nm and 259.940 nm and averaged for data usage. Please note that the general precision of ICP-OES measurements is in the range of 10 ppb for relatively low Fe concentrations (e.g., <1 ppm).[56] In addition, we suspect a significantly larger error at higher Fe concentrations, as the Fe concentration approaches the solubility limit and can easily exceed the limit when the electrolyte samples cool down.

RESOURCE AVAILABILITY

Lead contact

Further information and requests for resources and reagents should be directed to and will be fulfilled by the lead contact, Anna K. Mechler (anna.mechler@avt.rwth-aachen.de).

Materials availability

For resources used in this manuscript, please refer to Table S1.

Data and code availability

- All data reported have been deposited at the Zenodo repository and are publicly available as of the date of publication under https://doi.org/10.5281/zenodo.16140856.
- This paper does not report original code.
- Any additional information required to reanalyze the data reported in this paper is available from the lead contact upon request.

ACKNOWLEDGMENTS

We acknowledge the financial support by the German Federal Ministry of Research, Technology, and Space (BMFTR project "PrometH2eus," FKZ 03HY105A & 03HY105H). Furthermore, we thank our industry partner De Nora Deutschland GmbH, particularly Dr. Praveen V. Narangoda, Dr. Emanuele Instuli, and Dr. Robert Scannell, for providing electrode materials and guiding us through this project. We would also like to thank Stefanie Khan (AVT.ERT) and Alina Tran (AVT.ERT) for conducting electrochemical measurements, as well as Malgorzata Kwiatkowska (AVT.ERT) and Karin Faensen (AVT.CVT) for conducting ICP-OES and SEM-EDX measurements, respectively. Open access funding is enabled and organized by Projekt DEAL.

AUTHOR CONTRIBUTIONS

Conceptualization, N.T., Y.D., and A.K.M.; methodology, N.T., Y.D., and A.K.M.; data curation and investigation, N.T., Y.D., and H.M.F.; writing – original draft, N.T.; writing – review & editing, Y.D., H.M.F., V.S., J.P.H., and A.K.M.; funding acquisition, V.S., J.P.H., and A.K.M.; resources, V.S., J.P.H., and A.K.M.; and supervision V.S., J.P.H., and A.K.M.

DECLARATION OF INTERESTS

The authors declare no competing interests.

DECLARATION OF GENERATIVE AI AND AI-ASSISTED TECHNOLOGIES IN THE WRITING PROCESS

During the preparation of this work, the authors used chatgpt.com and chat.kiconnect.nrw in order to paraphrase and improve self-generated text. After using this tool or service, the authors reviewed and edited the content as needed and take full responsibility for the content of the publication.

SUPPLEMENTAL INFORMATION

Supplemental information can be found online at https://doi.org/10.1016/j.xcrp.2026.103138.

Received: August 18, 2025
Revised: November 11, 2025
Accepted: January 19, 2026
Published: February 18, 2026

REFERENCES

1. Wang, S., Lu, A., and Zhong, C.J. (2021). Hydrogen production from water electrolysis: role of catalysts. Nano Converg. *8*, 4. https://doi.org/10.1186/s40580-021-00254-x.
2. Grigoriev, S.A., Fateev, V.N., Bessarabov, D.G., and Millet, P. (2020). Current status, research trends, and challenges in water electrolysis science and technology. Int. J. Hydrogen Energy *45*, 26036–26058. https://doi.org/10.1016/j.ijhydene.2020.03.109.
3. Guo, Y., Li, G., Zhou, J., and Liu, Y. (2019). Comparison between Hydrogen Production by Alkaline Water Electrolysis and Hydrogen Production by PEM Electrolysis, *042022* (IOP Publishing). https://doi.org/10.1088/1755-1315/371/4/042022.
4. Schalenbach, M., Zeradjanin, A.R., Kasian, O., Cherevko, S., and Mayrhofer, K.J. (2018). A Perspective on Low-Temperature Water Electrolysis – Challenges in Alkaline and Acidic Technology. Int. J. Electrochem. Sci. *13*, 1173–1226. https://doi.org/10.20964/2018.02.26.
5. Jung, S., McCrory, C.C.L., Ferrer, I.M., Peters, J.C., and Jaramillo, T.F. (2016). Benchmarking nanoparticulate metal oxide electrocatalysts for the alkaline water oxidation reaction. J. Mater. Chem. A Mater. *4*, 3068–3076. https://doi.org/10.1039/c5ta07586f.
6. Lu, F., Zhou, M., Zhou, Y., and Zeng, X. (2017). First-Row Transition Metal Based Catalysts for the Oxygen Evolution Reaction under Alkaline Conditions: Basic Principles and Recent Advances. Small *13*, 1701931. https://doi.org/10.1002/smll.201701931.
7. Ďurovič, M., Hnát, J., and Bouzek, K. (2021). Electrocatalysts for the hydrogen evolution reaction in alkaline and neutral media. A comparative review. J. Power Sources *493*, 229708. https://doi.org/10.1016/j.jpowsour.2021.229708.
8. Peugeot, A., Creissen, C.E., Karapinar, D., Tran, H.N., Schreiber, M., and Fontecave, M. (2021). Benchmarking of oxygen evolution catalysts on porous nickel supports. Joule *5*, 1281–1300. https://doi.org/10.1016/j.joule.2021.03.022.
9. Anantharaj, S., Kundu, S., and Noda, S. (2021). "The Fe Effect": A review unveiling the critical roles of Fe in enhancing OER activity of Ni and Co based catalysts. Nano Energy *80*, 105514. https://doi.org/10.1016/j.nanoen.2020.105514.
10. Mauer, A.E., Kirk, D.W., and Thorpe, S.J. (2007). The role of iron in the prevention of nickel electrode deactivation in alkaline electrolysis. Electrochim. Acta *52*, 3505–3509. https://doi.org/10.1016/j.electacta.2006.10.037.
11. Zhou, P., Bai, H., Feng, J., Liu, D., Qiao, L., Liu, C., Wang, S., and Pan, H. (2023). Recent progress on bulk Fe-based alloys for industrial alkaline water electrolysis. J. Mater. Chem. A Mater. *11*, 1551–1574. https://doi.org/10.1039/d2ta09052j.
12. Bukowski, A., Olu, P.-Y., Gering, A., Chatenet, M., and Bonnefont, A. (2024). Dissolved iron in alkaline media: Techniques and insights for understanding its effects on water-splitting reactions. Curr. Opin. Electrochem. *47*, 101568. https://doi.org/10.1016/j.coelec.2024.101568.
13. de Groot, M.T. (2023). Alkaline water electrolysis: with or without iron in the electrolyte? Curr. Opin. Chem. Eng. *42*, 100981. https://doi.org/10.1016/j.coche.2023.100981.
14. Riley, M.A., and Moran, P.J. (1986). The Influence of Iron Deposition on the Voltage-Time Behavior of Nickel Cathodes in Alkaline Water Electrolysis. J. Electrochem. Soc. *133*, 760–761. https://doi.org/10.1149/1.2108670.
15. Abouatallah, R.M., Kirk, D.W., and Graydon, J.W. (2002). Long-term electrolytic hydrogen permeation in nickel and the effect of vanadium species addition. Electrochim. Acta *47*, 2483–2494. https://doi.org/10.1016/S0013-4686(02)00108-1.
16. Soares, D.M., Teschke, O., and Torriani, I. (1992). Hydride effect on the kinetics of the hydrogen evolution reaction on nickel cathodes in alkaline media. J. Electrochem. Soc. *139*, 98–105. https://doi.org/10.1149/1.2069207.
17. Brossard, L. (1991). Electrocatalytic performance for alkaline water electrolysis of Ni electrodes electrocoated with Fe or Fe/Mo. Int. J. Hydrogen Energy *16*, 13–21. https://doi.org/10.1016/0360-3199(91)90056-O.
18. Brossard, L., and Huot, J.-Y. (1991). In situ activation of cathodes during alkaline water electrolysis by dissolved iron and molybdenum species. J. Appl. Electrochem. *21*, 508–515. https://doi.org/10.1007/BF01018603.
19. Huot, J., and Brossard, L. (1987). Time dependence of the hydrogen discharge at 70 C on nickel cathodes. Int. J. Hydrogen Energy *12*, 821–830. https://doi.org/10.1016/0360-3199(87)90103-0.
20. Spanos, I., Masa, J., Zeradjanin, A., and Schlögl, R. (2021). The Effect of Iron Impurities on Transition Metal Catalysts for the Oxygen Evolution Reaction in Alkaline Environment: Activity Mediators or Active Sites? Catal. Letters *151*, 1843–1856. https://doi.org/10.1007/s10562-020-03478-4.
21. Bao, F., Kemppainen, E., Dorbandt, I., Xi, F., Bors, R., Maticiuc, N., Wenisch, R., Bagacki, R., Schary, C., Michalczik, U., et al. (2021). Host, Suppressor, and Promoter—The Roles of Ni and Fe on Oxygen Evolution Reaction Activity and Stability of NiFe Alloy Thin Films in Alkaline Media. ACS Catal. *11*, 10537–10552. https://doi.org/10.1021/acscatal.1c01190.
22. Bhandari, S., Narangoda, P.V., Mogensen, S.O., Tesch, M.F., and Mechler, A.K. (2022). Effect of Experimental Parameters on the Electrocatalytic Performance in Rotating Disc Electrode Measurements: Case Study of Oxygen Evolution on Ni–Co-Oxide in Alkaline Media. Chemelectrochem *9*, e202200479. https://doi.org/10.1002/celc.202200479.
23. Etxebarria, A., Lopez Luna, M., Martini, A., Hejral, U., Rüscher, M., Zhan, C., Herzog, A., Jamshaid, A., Kordus, D., Bergmann, A., et al. (2024). Effect of Iron Doping in Ordered Nickel Oxide Thin Film Catalyst for the Oxygen Evolution Reaction. ACS Catal. *14*, 14219–14232. https://doi.org/10.1021/acscatal.4c02572.
24. Trotochaud, L., Young, S.L., Ranney, J.K., and Boettcher, S.W. (2014). Nickel–Iron Oxyhydroxide Oxygen-Evolution Electrocatalysts: The Role of Intentional and Incidental Iron Incorporation. J. Am. Chem. Soc. *136*, 6744–6753. https://doi.org/10.1021/ja502379c.
25. Chung, D.Y., Lopes, P.P., Farinazzo Bergamo Dias Martins, P., He, H., Kawaguchi, T., Zapol, P., You, H., Tripkovic, D., Strmcnik, D., Zhu, Y., et al. (2020). Dynamic stability of active sites in hydr(oxy)oxides for the oxygen evolution reaction. Nat. Energy *5*, 222–230. https://doi.org/10.1038/s41560-020-0576-y.

26. Kuai, C., Xi, C., Hu, A., Zhang, Y., Xu, Z., Nordlund, D., Sun, C.-J., Cadigan, C.A., Richards, R.M., Li, L., et al. (2021). Revealing the Dynamics and Roles of Iron Incorporation in Nickel Hydroxide Water Oxidation Catalysts. J. Am. Chem. Soc. *143*, 18519–18526. https://doi.org/10.1021/jacs.1c07975.

27. Feng, C., Wang, F., Liu, Z., Nakabayashi, M., Xiao, Y., Zeng, Q., Fu, J., Wu, Q., Cui, C., Han, Y., et al. (2021). A self-healing catalyst for electrocatalytic and photoelectrochemical oxygen evolution in highly alkaline conditions. Nat. Commun. *12*, 5980. https://doi.org/10.1038/s41467-021-26281-0.

28. Kang, S., Im, C., Spanos, I., Ham, K., Lim, A., Jacob, T., Schlögl, R., and Lee, J. (2022). Durable Nickel-Iron (Oxy)hydroxide Oxygen Evolution Electrocatalysts through Surface Functionalization with Tetraphenylporphyrin. Angew. Chem. Int. Ed. Engl. *61*, e202214541. https://doi.org/10.1002/anie.202214541.

29. Deo, Y., Thissen, N., Seidl, V., Gallenberger, J., Hoffmann, J., Hofmann, J.P., Etzold, B.J.M., and Mechler, A.K. (2024). Thin Nickel Coatings on Stainless Steel for Enhanced Oxygen Evolution and Reduced Iron Leaching in Alkaline Water Electrolysis. Electrochem. Sci. Adv. *5*, e202400023. https://doi.org/10.1002/elsa.202400023.

30. Channei, D., Phanichphant, S., Nakaruk, A., Mofarah, S., Koshy, P., and Sorrell, C. (2017). Aqueous and Surface Chemistries of Photocatalytic Fe-Doped CeO2 Nanoparticles. Catalysts *7*, 45. https://doi.org/10.3390/catal7020045.

31. Demnitz, M., Lamas, Y.M., Garcia Barros, R.L., de Leeuw den Bouter, A., van der Schaaf, J., and Theodorus de Groot, M. (2024). Effect of iron addition to the electrolyte on alkaline water electrolysis performance. iScience *27*, 108695. https://doi.org/10.1016/j.isci.2023.108695.

32. Abdel Haleem, A., Nagasawa, K., Kuroda, Y., Nishiki, Y., Zaenal, A., and Mitsushima, S. (2021). A New Accelerated Durability Test Protocol for Water Oxidation Electrocatalysts of Renewable Energy Powered Alkaline Water Electrolyzers. Electrochemistry *89*, 186–191. https://doi.org/10.5796/electrochemistry.20-00156.

33. Uchino, Y., Kobayashi, T., Hasegawa, S., Nagashima, I., Sunada, Y., Manabe, A., Nishiki, Y., and Mitsushima, S. (2017). Relationship Between the Redox Reactions on a Bipolar Plate and Reverse Current After Alkaline Water Electrolysis. Electrocatalysis *9*, 67–74. https://doi.org/10.1007/s12678-017-0423-5.

34. Holmin, S., Näslund, L.Å., Ingason, Á.S., Rosen, J., and Zimmerman, E. (2014). Corrosion of ruthenium dioxide based cathodes in alkaline medium caused by reverse currents. Electrochim. Acta *146*, 30–36. https://doi.org/10.1016/j.electacta.2014.09.024.

35. Ishikawa, K., Yoshioka, T., Sato, T., and Okuwaki, A. (1997). Solubility of hematite in LiOH, NaOH and KOH solutions. Hydrometallurgy *45*, 129–135. https://doi.org/10.1016/S0304-386X(96)00068-0.

36. Thissen, N., Hoffmann, J., Tigges, S., Vogel, D.A.M., Thoede, J.J., Khan, S., Schmitt, N., Heumann, S., Etzold, B.J.M., and Mechler, A.K. (2023). Industrially Relevant Conditions in Lab-Scale Analysis for Alkaline Water Electrolysis. Chemelectrochem *11*, e202300432. https://doi.org/10.1002/celc.202300432.

37. Galkina, I., Faid, A.Y., Jiang, W., Scheepers, F., Borowski, P., Sunde, S., Shviro, M., Lehnert, W., and Mechler, A.K. (2024). Stability of Ni-Fe-Layered Double Hydroxide Under Long-Term Operation in AEM Water Electrolysis. Small *20*, e2311047. https://doi.org/10.1002/smll.202311047.

38. Iranzo, A., and Mulder, F.M. (2021). Nickel-iron layered double hydroxides for an improved Ni/Fe hybrid battery-electrolyser. Mater. Adv. *2*, 5076–5088. https://doi.org/10.1039/d1ma00024a.

39. Klaus, S., Cai, Y., Louie, M.W., Trotochaud, L., and Bell, A.T. (2015). Effects of Fe Electrolyte Impurities on Ni(OH)2/NiOOH Structure and Oxygen Evolution Activity. J. Phys. Chem. C *119*, 7243–7254. https://doi.org/10.1021/acs.jpcc.5b00105.

40. Mattinen, M., Schröder, J., D'Acunto, G., Ritala, M., Jaramillo, T.F., Stevens, M.B., and Bent, S.F. (2024). Dynamics of precatalyst conversion and iron incorporation in nickel-based alkaline oxygen evolution reaction catalysts. Cell Rep. Phys. Sci. *5*, 102284. https://doi.org/10.1016/j.xcrp.2024.102284.

41. Gohlke, C., Gallenberger, J., Niederprüm, N., Ingendae, H., Kautz, J., Hofmann, J.P., and Mechler, A.K. (2024). Boosting the Oxygen Evolution Reaction Performance of Ni-Fe-Electrodes by Tailored Conditioning. Chemelectrochem *11*, e202400318. https://doi.org/10.1002/celc.202400318.

42. Pourbaix, M. (1966). Atlas of Electrochemical Equilibria in Aqueous Solutions. Science *154*, 1537.

43. Beverskog, B., and Puigdomenech, I. (1996). Revised pourbaix diagrams for iron at 25–300 C. Corros. Sci. *38*, 2121–2135. https://doi.org/10.1016/S0010-938X(96)00067-4.

44. Liu, P., Wang, J., Wang, X., Liu, L., Yan, X., Wang, H., Lu, Q., Wang, F., and Ren, Z. (2024). A superhydrophilic NiFe electrode for industrial alkaline water electrolysis. Int. J. Hydrogen Energy *49*, 285–294. https://doi.org/10.1016/j.ijhydene.2023.07.253.

45. Han, W.-B., Kim, I.-S., Kim, M., Cho, W.C., Kim, S.-K., Joo, J.H., Lee, Y.-W., Cho, Y., Cho, H.-S., and Kim, C.-H. (2021). Directly sputtered nickel electrodes for alkaline water electrolysis. Electrochim. Acta *386*, 138458. https://doi.org/10.1016/j.electacta.2021.138458.

46. Schalenbach, M., Kasian, O., and Mayrhofer, K.J.J. (2018). An alkaline water electrolyzer with nickel electrodes enables efficient high current density operation. Int. J. Hydrogen Energy *43*, 11932–11938. https://doi.org/10.1016/j.ijhydene.2018.04.219.

47. Industrie De Nora S.p.A. (2016). De Nora electrodic package for Alkaline Water Electrolysis. www.denora.com/applications/H2-production-by-water-electrolysis.

48. Lin, B.-L., Chen, X., Niu, B.-T., Lin, Y.-T., Chen, Y.-X., and Lin, X.-M. (2024). The Research Progress of Ruthenium-Based Catalysts for the Alkaline Hydrogen Evolution Reaction in Water Electrolysis. Catalysts *14*, 671. https://doi.org/10.3390/catal14100671.

49. Becker, H., Murawski, J., Shinde, D.V., Stephens, I.E.L., Hinds, G., and Smith, G. (2023). Impact of impurities on water electrolysis: a review. Sustain. Energy Fuels *7*, 1565–1603. https://doi.org/10.1039/d2se01517j.

50. Marquez, R.A., Kalokowski, E., Espinosa, M., Bender, J.T., Son, Y.J., Kawashima, K., Chukwuneke, C.E., Smith, L.A., Celio, H., Dolocan, A., et al. (2024). Transition metal incorporation: electrochemical, structure, and chemical composition effects on nickel oxyhydroxide oxygen-evolution electrocatalysts. Energy Environ. Sci. *17*, 2028–2045. https://doi.org/10.1039/D3EE03617K.

51. Jerkiewicz, G. (2020). Standard and Reversible Hydrogen Electrodes: Theory, Design, Operation, and Applications. ACS Catal. *10*, 8409–8417. https://doi.org/10.1021/acscatal.0c02046.

52. Tsotridis, G., and Pilenga, A. (2021). EU Harmonised Protocols for Testing of Low Temperature Water Electrolysers (European Comission). https://doi.org/10.2760/58880.

53. Fairley, N., Fernandez, V., Richard-Plouet, M., Guillot-Deudon, C., Walton, J., Smith, E., Flahaut, D., Greiner, M., Biesinger, M., Tougaard, S., et al. (2021). Systematic and collaborative approach to problem solving using X-ray photoelectron spectroscopy. Appl. Surf. Sci. Adv. *5*, 100112. https://doi.org/10.1016/j.apsadv.2021.100112.

54. Crist, B. (1999). Fundamental XPS Data from Pure Elements (Pure Oxides and Chemical Compounds, XPS International Inc.).

55. Crist, B.V. (2000). Handbook of Monochromatic XPS Spectra: The Elements of Native Oxides (John Wiley & Sons).

56. Chen, R., Hung, S.F., Zhou, D., Gao, J., Yang, C., Tao, H., Yang, H.B., Zhang, L., Zhang, L., Xiong, Q., et al. (2019). Layered Structure Causes Bulk NiFe Layered Double Hydroxide Unstable in Alkaline Oxygen Evolution Reaction. Adv. Mater. *31*, e1903909. https://doi.org/10.1002/adma.201903909.